RESEARCH ARTICLE

Check for updates

Regulation of excited-state properties of dibenzothiophene-based fluorophores for realizing efficient deep-blue and HLCT-sensitized OLEDs†

Jichen Lv,[a] Yumiao Huo, [ID][d] Shu Xiao,[b] Zhennan Zhao,[c] Ling Peng, [ID][a] Yuchao Liu,[a] Zhongjie Ren, [ID][c] Dongge Ma, [ID][b] Shian Ying [ID] *[ab] and Shouke Yan [ID] *[ac]

Efficient and multifunctional deep-blue organic luminescent materials are in great demand for the development of organic light-emitting diodes (OLEDs) in the application of ultrahigh-definition displays with a wide color gamut and highly saturated color. Herein, two deep-blue hybridized local and charge-transfer (HLCT) dibenzothiophene-phenanthroimidazole fluorophores were designed and synthesized by regulating the electron-withdrawing abilities of anchoring groups (phenyl and cyanophenyl) at the phenanthroimidazole unit. Computational and photophysical investigations reveal that the introduction of a cyano-group can finely modulate the component of excited states while maintaining similar luminescence colors. Consequently, the resulting non-doped devices show electroluminescence peaks at 451 and 452 nm with the Commission Internationale de l'Éclairage (CIE) coordinates of (0.152, 0.067) and (0.153, 0.064). Based on HLCT-sensitized fluorescence and phosphorescence, high external quantum efficiencies (EQEs) of 7.08% and 27.30% and low efficiency roll-off are achieved concurrently at low doping concentrations. Moreover, a high-performance hybrid warm-white OLED with an EQE of 26.56% is obtained using the incomplete energy transfer process.

Introduction

Organic luminescent materials (OLMs) have attracted widespread attention in the application of organic light-emitting diodes (OLEDs), organic lasers, organic light-emitting transistors (OFETs), biological imaging devices, chemical sensors, and so on.[1–4] Especially in recent years, the rapid development of OLEDs in full-color displays (televisions, smartphones, smart watches, *etc.*) has pushed up demand for OLMs. In terms of three primary-color (red, green, and blue) OLEDs, red and green OLEDs based on phosphorescent metallic complexes have met

the market demand in the device efficiency and operating lifetime. However, blue OLEDs, especially deep-blue OLEDs that matched the Commission international de I'Eclairage (CIE) coordinate of $CIE_y < 0.08$ are far behind them,[5–7] resulting from their inherent wide bandgap feature. Though traditional blue fluorescent emitters possess excellent device stability, only 25 percent of electrogenerated excitons (singlet excitons) can be harvested for emitting light, and others (triplet excitons) are turned into heat and other forms of energy to be dissipated, leading to a low electroluminescence (EL) performance with the upper limit of external quantum efficiency (EQE) of ∼5%. Blue phosphorescent and thermally activated delayed fluorescent (TADF) emitters can harvest both singlet and triplet excitons, realizing 100% theoretical internal quantum efficiency, but they have to be doped into a suitable host with a triplet state energy higher than that of emitters for weakening concentration quenching and triplet exciton annihilation effects.[8–11] In addition, the dependable deep-blue emission and color purity of phosphorescent and TADF emitters still remain unsatisfactory owing to their relatively strong metal–ligand charge-transfer (MLCT) and charge-transfer (CT) excited states. What is more, an efficient deep-blue material should not only serve as an emitter for full-color displays to

[a] *Key Laboratory of Rubber-Plastics, Ministry of Education, School of Polymer Science and Engineering, Qingdao University of Science and Technology, Qingdao 266042, P. R. China. E-mail: shian0610@126.com, skyan@mail.buct.edu.cn*

[b] *Institute of Polymer Optoelectronic Materials and Devices, State Key Laboratory of Luminescent Materials and Devices, South China University of Technology, Guangzhou 510640, P. R. China*

[c] *College of Materials Science and Engineering, Shandong University of Science and Technology, Qingdao 266590, P. R. China*

[d] *State Key Laboratory of Chemical Resource Engineering, College of Materials Science and Engineering, Beijing University of Chemical Technology, Beijing 100029, P. R. China*

decrease the power loss but also be used as a host for white OLEDs (WOLEDs) to generate longer wavelength emissions in lighting applications.[12,13] Until now, it is still an urgent demand for the development and application of OLED technology to develop such multifunctional deep-blue materials with CIEy < 0.08.

The dibenzothiophene (DBT) group with a rigid and planar molecular structure possesses flexible structural modification, excellent thermal stability, a narrow emission spectrum, a high triplet energy level, and somewhat bipolar-transporting properties,[14,15] and has been utilized in a wide variety of optoelectronic applications, including OLEDs, OFETs, and polymer solar cells (PSCs). Moreover, the heavy atom effect of sulfur can enhance the spin–orbit coupling (SOC), which can effectively modulate the intersystem crossing (ISC) and reversed intersystem crossing (RISC) processes. However, most of the reported DBT derivatives were used as the host for phosphorescent and TADF dopants[16–27] and connected with acceptor or donor units to construct electron- or hole-transporting materials,[28–30] and only a few of them were used as yellow, green, and blue emitters in OLEDs.[26,31,32] For example, Guo *et al.* developed a series of green and yellow TADF emitters with DBT as a donor unit, achieving high EQEs of over 9% in the non-doped devices.[33,34] Tang and co-workers synthesized a dual-emitting-core compound (2DBT-BZ-2Cz) with green emission, demonstrating a current efficiency of 20.7 cd A^{-1} in a solution-processed OLED.[35] Xia *et al.* reported a dibenzothiophene-triphenylamine derivative (ST-G1) with an EL peak at 445 nm, realizing a current efficiency of 0.48 cd A^{-1}.[36] Sim *et al.* achieved pyrene derivatives (DDPI and DPPI) including the dibenzothiophene moiety, realizing an EQE of 3.07% and CIE coordinates of (0.16, 0.16).[37] Lee and co-workers developed an *N,N*-diphenyl aminofluorene styryl emitter with DBT as the end group, showing a current efficiency of 8.11 cd A^{-1} and CIE coordinates of (0.154, 0.163) in the doped device with typical triplet–triplet annihilation (TTA) molecule ADN as the host.[38] Yao and Tang reported two blue fluorescent DBT-bridged molecules (D1 and PISF) with EQE values of 1.7% and 2.60% in non-doped devices, showing the CIE coordinates of (0.17, 0.09) and (0.16, 0.09).[39,40] The DBT-based fluorophores with CIEy < 0.08 have not been reported previously in non-doped OLEDs. Moreover, there is still much room for further improving the EL efficiency and multifunction through molecular and device engineering.

It is known that phenanthroimidazole (PI) with suitable energy levels, high luminous efficiency, and bipolar-transporting characteristics is a representative building block for blue materials. In this work, two novel deep-blue DBT-PI fluorophores (**PIS** and **CNPIS**) were designed and synthesized by regulating the electron-withdrawing ability of anchoring groups (phenyl and cyanophenyl) at the N1 position of the PI unit. Because of the large dihedral angles, cyano modification has a small effect on the emission color, but it reduces the lowest-excited singlet–triplet (S$_1$–T$_1$) energy gap (ΔE_{ST}) and enhances the CT state components in the S$_1$ state. As a result, utilizing the phenyl-substituted **PIS** as the sensitizer in OLEDs,

high EQEs of 7.08%, 27.30%, and 26.56% and low efficiency roll-off at high luminance are achieved simultaneously.

Experimental methods

Synthesis and characterization of materials

Synthesis of 2-(4-(dibenzo[*b,d*]thiophen-4-yl)phenyl)-1-phenyl-1*H*-phenanthro[9,10-*d*]imidazole (PIS). Under a nitrogen atmosphere, 2-(4-bromophenyl)-1-phenyl-1*H*-phenanthro[9,10-*d*]imidazole (2.25 g, 5 mmol) dibenzo[*b,d*]thiophen-4-ylboronic acid (1.37 g, 6 mmol), Pd(PPh$_3$)$_4$ (0.23 g, 0.2 mmol), CH$_3$CH$_2$OH (10 mL), toluene (30 mL) and 2 M solution of K$_2$CO$_3$ in water (10 mL) were added to a 100 mL two-neck round-bottom flask and refluxed at 110 °C for 24 h. After cooling down, the reaction mixture was extracted three times using CH$_2$Cl$_2$ and water. The organic layer was dried with anhydrous MgSO$_4$, filtered, and evaporated under reduced pressure. The crude product was purified by silica-gel column chromatography using petroleum/CH$_2$Cl$_2$ (1/1, v/v) as the solvent and finally further purified by a multi-temperature-zone sublimator to give a white solid (1.65 g, 60%). ^{1}H NMR (500 MHz, CDCl$_3$, δ ppm): 8.96 (d, J = 7.9 Hz, 1H), 8.75 (dd, J = 28.5, 8.3 Hz, 2H), 8.24–8.03 (m, 2H), 7.86–7.81 (m, 1H), 7.81–7.72 (m, 3H), 7.67 (dd, J = 20.0, 8.1 Hz, 6H), 7.58 (d, J = 7.2 Hz, 2H), 7.52 (t, J = 7.6 Hz, 2H), 7.49–7.42 (m, 3H), 7.28 (t, J = 8.1 Hz, 1H), 7.21 (d, J = 8.2 Hz, 1H). ^{13}C NMR (126 MHz, CDCl$_3$, δ ppm): 150.53, 141.04, 139.64, 138.91, 138.55, 136.46, 136.46, 136.32, 135.80, 130.38, 130.03, 129.81, 129.48, 129.29, 128.47, 128.23, 127.45, 126.98, 126.41, 125.80, 125.20, 125.06, 124.53, 124.25, 123.26, 123.18, 122.96, 122.72, 121.83, 121.01, 120.82. TOF-MS(ESI) m/z calcd. for C$_{39}$H$_{24}$N$_2$S: 552.1660; [M + H]$^+$ found: 553.1734.

Synthesis of 4-(2-(4-(dibenzo[*b,d*]thiophen-4-yl)phenyl)-1*H*-phenanthro[9,10-*d*]imidazol-1-yl)benzonitrile (CNPIS). Under a nitrogen atmosphere, 4-(2-(4-bromophenyl)-1*H*-phenanthro-[9,10-*d*]imidazol-1-yl)benzonitrile (2.37 g, 5 mmol) dibenzo-[*b,d*]thiophen-4-ylboronic acid (1.37 g, 6 mmol), Pd(PPh$_3$)$_4$ (0.23 g, 0.2 mmol), CH$_3$CH$_2$OH (10 mL), toluene (30 mL) and 2 M solution of K$_2$CO$_3$ in water (10 mL) were added to a 100 mL two-neck round-bottom flask and refluxed at 110 °C for 24 h. After cooling down, the reaction mixture was extracted using CH$_2$Cl$_2$ and water. The organic layer was dried using anhydrous MgSO$_4$, filtered, and evaporated under reduced pressure. The crude product was purified by silica-gel column chromatography using petroleum/CH$_2$Cl$_2$ (2/3, v/v) as the solvent and finally further purified by a multi-temperature-zone sublimator to give a white solid (1.51 g, 52%). ^{1}H NMR (400 MHz, CDCl$_3$, δ ppm): 8.92 (d, J = 7.9 Hz, 1H), 8.84–8.77 (m, 1H), 8.71 (d, J = 8.2 Hz, 1H), 8.22–8.11 (m, 2H), 8.00–7.92 (m, 2H), 7.89–7.82 (m, 1H), 7.80–7.61 (m, 8H), 7.61–7.51 (m, 2H), 7.51–7.42 (m, 3H), 7.33 (ddd, J = 8.3, 7.0, 1.2 Hz, 1H), 7.13 (dd, J = 8.3, 1.3 Hz, 1H). ^{13}C NMR (101 MHz, CDCl$_3$, δ ppm): 158.10, 153.52, 148.58, 143.11, 139.54, 138.49, 136.55, 134.26, 131.74, 130.89, 130.44, 130.07, 129.71, 128.59, 128.55, 127.77, 127.11, 127.04, 126.74, 126.36, 125.62, 125.29, 124.64, 124.61, 123.30, 123.15, 122.81, 122.45, 121.89, 121.07, 120.67, 117.83. TOF-MS(ESI) m/z calcd. for C$_{40}$H$_{23}$N$_3$S: 577.1613; [M + H]$^+$ found: 578.1668.

Results and discussion
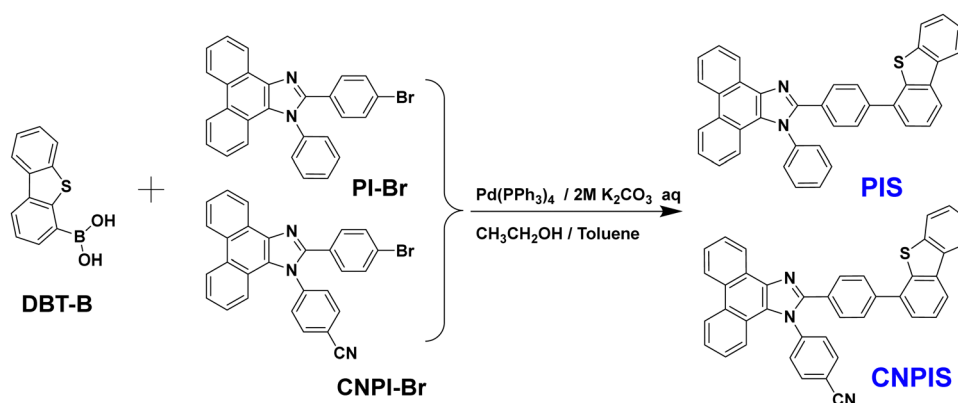
Synthesis and thermal properties

As shown in Scheme 1, the target compounds (**PIS** and **CNPIS**) were synthesized from the Suzuki-coupling procedure between dibenzo[*b*,*d*]thiophen-4-yl boronic acid (**DBT-B**) and 2-(4-bromophenyl)-1-phenyl-1*H*-phenanthro[9,10-*d*]imidazole (PI-Br) and 4-(2-(4-bromophenyl)-1*H*-phenanthro[9,10-*d*]imidazol-1-yl)-benzonitrile (**CNPI-Br**), where **PI-Br** and **CNPI-Br** were obtained based on different literature studies.[41–43] After purifying by vacuum sublimation, the structures of **PIS** and **CNPIS** were confirmed by NMR spectra and mass spectrometry. Their detailed synthesis and characterization are shown in the Experimental Section. Thermal gravimetric analysis (TGA) and differential scanning calorimetry (DSC) were performed to investigate the thermal stability of **PIS** and **CNPIS**. As depicted in Fig. S1 (ESI†) and Table 1, decomposition temperatures (T_ds) with a 5% weight loss were 404 and 423 °C for **PIS** and **CNPIS**, respectively. The glass-transition temperature (T_g) of **PIS** was measured to be 127 °C, while no obvious T_g was found upon second heating for **CNPIS**.

Photophysical properties

Ultraviolet-visible (UV-vis) absorption and photoluminescence (PL) spectra of target materials were recorded to investigate their photophysical properties. As shown in Fig. 1 and Table 1, **PIS** and **CNPIS** show similar absorption peaks' location at ~337 and ~362 nm in the dilute tetrahydrofuran solution, corresponding to the π–π* transition of the substituent on the 2-imidazole position to the PI unit and π–π* transition of the PI unit.[31,44] The optical bandgaps (E_gs) of **PIS** and **CNPIS** can be calculated to be 3.23 and 3.22 eV from the absorption onset, respectively. The PL emission peak of **PIS** is located at 408 nm, while **CNPIS** shows an obvious red-shift emission with a maximum peak of 423 nm due to the intramolecular charge transfer (ICT) effect induced by cyano-substitution. In the neat film, due to intermolecular interactions, both of them exhibit red-shifted emission but are still located at the deep-blue region with peaks of 432 and 438 nm for **PIS** and **CNPIS**, respectively. The absolute PL quantum yield (PLQY) of the **PIS** film is 49.70%, higher than that of **CNPIS** (30.37%).

To further study the property of excited states of **PIS** and **CNPIS**, their solvatochromic effects in different solvents were measured. As shown in Fig. S2, S3, and Tables S1, S2 (ESI†), by increasing the solvent polarity from hexane to acetonitrile, the absorption spectra are insensitive to the solvent polarity, while the PL spectra show a notable red shift from 386 to 418 nm for **PIS** and from 404 to 434 nm for **CNPIS**, manifesting the presence of the ICT excited state. For **PIS** with phenyl modification at the N1 of the PI unit, the PL spectra feature a vibrational fine emission in low-polar solvents and convert to broad featureless emission in high-polar solvents. However, the cyanophenyl-substitution changes the spectral pattern that **CNPIS** displays broad and structureless characteristics in all the solvents, demonstrating that the introduction of a cyano-group can effectively regulate the component of excited states. As shown in Fig. S4 (ESI†), Stokes shift ($\nu_a - \nu_{PL}$) *versus* orientation polarizability (*f*) characteristics of **PIS** and **CNPIS** were fitted by the Lippert–Mataga model. **PIS** shows two section lines with the excited-state dipole moments (μ_es) of 8.66 and
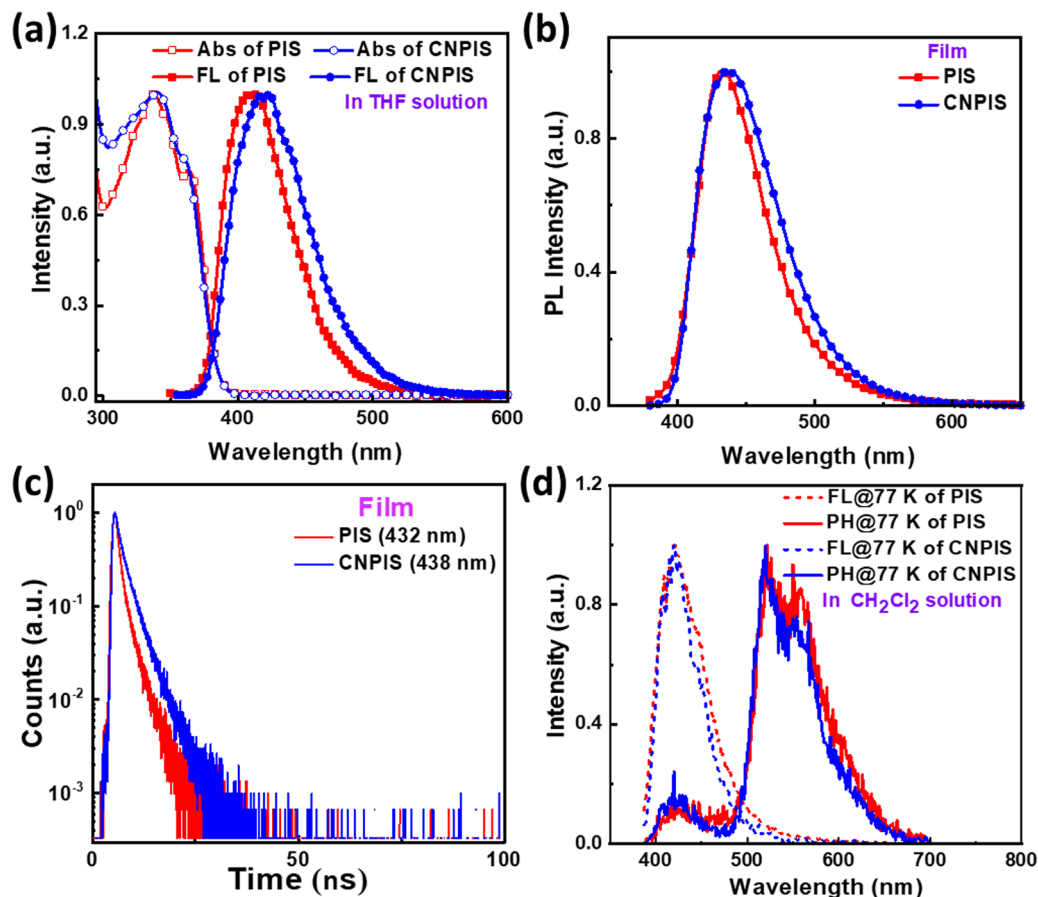
Scheme 1 The chemical equations for the synthesis of **PIS** and **CNPIS**.

Table 1 Photophysical, thermal and electrochemical properties of PIS and CNPIS are summarized

Compound	$\lambda_{F,S}{}^a$ [nm]	$\lambda_{F,F}{}^b$ [nm]	$E_S/E_T/\Delta E_{ST}{}^c$ [eV]	HOMO/LUMO/$E_g{}^d$ [eV]	$T_g/T_d{}^e$ [°C]	$\tau_F{}^b$ [ns]	$\Phi_{PL}{}^b$ [%]
PIS	408	432	2.94/2.38/0.56	−5.46/−2.23/3.23	127/404	1.19	49.70
CNPIS	423	438	2.95/2.39/0.56	−5.47/−2.25/3.22	—/423	2.26	30.37

[a] Measured in the THF solution (10^{-5} M) at room temperature. [b] Measured in the neat film at room temperature. [c] Measured in the DCM solution (10^{-5} M) at 77 K. [d] HOMO obtained from CV; LUMO energy calculated by adding the optical band gap to HOMO; E_g calculated form the absorption onset. [e] Measured by DSC and TGA.

This journal is © The Royal Society of Chemistry and the Chinese Chemical Society 2023

Mater. Chem. Front., 2023, **7**, 85–95 | 87

Fig. 1 (a) UV-vis absorption and emission spectra of **PIS** and **CNPIS** in dilute THF solution (10 μM) at room temperature. (b) Emission spectra of **PIS** and **CNPIS** thin films. (c) Transient PL decay spectra of **PIS** and **CNPIS** thin films. (d) Low-temperature fluorescence and phosphorescence spectra of **PIS** and **CNPIS** in the dichloromethane solution.

17.72 D in low- and high-polar solvents, belonging to typical hybridized local and charge-transfer (HLCT) characteristic. The well-fitted linear relationship with the μ_e of 12.43 D was achieved based on **CNPIS**, smaller than that of the typical CT molecule DMABN (23 D),[45] which may be regarded as a quasi-equivalent HLCT excited state.[42,46–50]

As depicted in Fig. S5 and Table S3 (ESI†), the mono-exponential decays with nanosecond-scale lifetimes in different solvents, further illustrating that there is only one excited state rather than a mixture of the LE and CT states, which is proved in the theoretical calculation section. The decay lifetimes of 1.19 and 2.26 ns for **PIS** and **CNPIS** were observed in the neat film (Fig. 1(c)). According to the PLQYs, the radiative transition rates (k_rs) of **PIS** and **CNPIS** can be calculated to be 4.18 and 1.34×10^8 s^{-1}. And non-radiative transition rates (k_{nr}s) were calculated to be 4.23 and 3.08×10^8 s^{-1}, respectively (summarized in Table S3, ESI†). From low-temperature fluorescence and phosphorescence spectra in the dichloromethane solution (Fig. 1(d)), the values of S$_1$ and T$_1$ energy levels were estimated to be 2.94/2.38 eV and 2.95/2.39 eV for **PIS** and **CNPIS**. Their ΔE_{ST} values are as high as 0.56 and 0.56 eV (Table 1). These results signify that the TADF process can be eliminated in this molecular system.

Theoretical calculation and electrochemical properties

The molecular geometries and electronic structures of **PIS** and **CNPIS** were investigated by density functional theory calculations using Gaussian 09 at the B3LYP/6-31G(d,p) level. As displayed in Fig. 2, both of them show similar twist angles
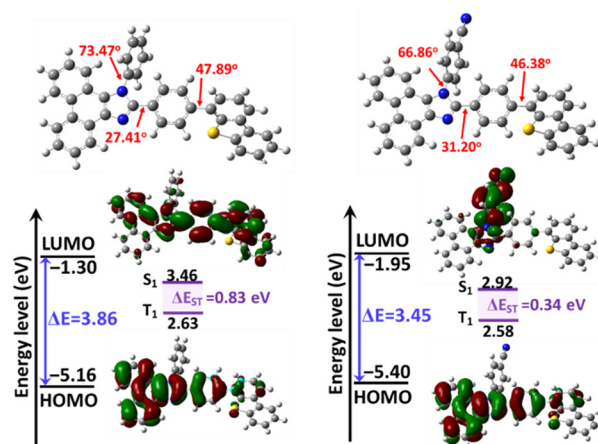
Fig. 2 Optimized geometries, HOMO and LUMO distributions and their energy levels of **PIS** and **CNPIS** computed at the B3LYP/6-31G (d,p) level.

(47.89° and 46.38°) between the PI unit and the DBT group, while the cyano-substituted **CNPIS** shows a relatively low twist angle between the cyanophenyl and imidazole ring. The introduction of the DBT group has a small effect on the twist angles between imidazole and adjacent benzene rings in the PI unit (Fig. S6, ESI†). It is noteworthy that both **PIS** and **CNPIS** show quite similar highest occupied molecular orbital (HOMO) distributions that are mainly distributed on phenanthrene, imidazole, and adjacent benzene rings and to a certain extent remain on the DBT unit. Nevertheless, their lowest unoccupied molecular orbital (LUMO) distributions are markedly different. The LUMO of **PIS** is delocalized almost on the entire molecular skeleton, while that of **CNPIS** is mainly located on the cyanophenyl and adjacent imidazole ring due to the strong electron-withdrawing ability of the cyano group. Fascinatingly, LUMO+1 of **CNPIS** is located on the whole PI-DBT framework, which is similar to the LUMO of **PIS** (Fig. S7, ESI†). The energy gap between HOMO and LUMO+1 of **CNPIS** (3.96 eV) is close to that of PIS (3.86 eV) from the HOMO to the LUMO. Due to efficient overlaps in the molecular orbitals for **PIS**, the transition from the HOMO to the LUMO is allowed. As for **CNPIS**, as a result of spatial separation between the HOMO and the LUMO, it is nearly forbidden in the photo-absorption process, whereas the transition from the HOMO to LUMO+1 should be allowed.[51] These results agree well with the approximately equal E_g between **PIS** and **CNPIS**. Their electrochemical properties were performed using cyclic voltammetry (CV) measurements. The HOMO levels of **PIS** and **CNPIS** were deduced to be −5.46 and −5.47 eV (Fig. S8, ESI†), and the LUMO levels were computed to be −2.23 and −2.25 eV according to the formula: $E_{LUMO} = E_{HOMO} + E_g$.

For gaining an in-depth understanding of the influences of the cyano-group on excited state properties, calculation of natural transition orbitals (NTOs) of **PIS** and **CNPIS** was further carried out. As shown in Fig. S9 and S10 (ESI†), during the $S_0 \rightarrow S_1$ transition of **PIS**, the hole is mainly located on the PI unit and to some extent dispersed in the DBT group, while the particle is mainly distributed in DBT and the adjacent benzene moieties. There are obvious spatial separations and partial overlaps between the hole and particle NTOs, belonging to

the typical HLCT state features. Additionally, it is also observed in the $S_0 \rightarrow S_2$ transition. For CN-modified **CNPIS**, the obvious CT transition with the particle located on benzonitrile and hole mainly delocalized in phenanthrene, imidazole, and adjacent benzene rings can be found in the $S_0 \rightarrow S_1$ transition, but the $S_0 \rightarrow S_2$ transition shows the distinct HLCT state. It can be seen from the calculated first-ten singlet and triplet excited states that a large ΔE_{ST} of 0.831 eV and the small energy gaps (0.0381/ −0.0941 eV) between S_1 and fifth/sixth triplet (T_5/T_6) excited states in molecule **PIS** can facilitate the high-lying reverse intersystem crossing (hRISC) process from T_5/T_6 to S_1. Though T_5 and T_6 exhibit LE-dominant character (Fig. S9, ESI†), according to Fermi's golden rule,[52] the large spin–orbit coupling (SOC) strengths of 0.636/0.709 cm^{-1} between S_1 and T_5/T_6 can effectively enhance the hRISC process (Fig. 3(a) and Table S4, S6, ESI†). As for **CNPIS**, S_1 and second triplet (T_2) states with prominent CT and HLCT characters (Fig. S10, ESI†) have the same transition configurations of 98.6% and 22.8% in HOMO → LUMO, respectively, according to El-Sayed' rule, which is beneficial to establish the transformation channel from triplet to singlet states.[53,54] In addition, the low energy gap of 0.0238 eV and a considerable SOC strength of 0.412 cm^{-1} between S_1 and T_2 can further accelerate the hRISC process (Fig. 3(b) and Table S5, ESI†). Therefore, the OLEDs with **PIS** and **CNPIS** as emitters are expected to exceed the theoretical upper bound of exciton utilization efficiency (EUE) based on traditional fluorescent OLEDs. By contrast, due to the larger ΔE_{ST} and SOC strength, the hRISC process of **PIS** should be more effective than that of **CNPIS**.

Deep-blue non-doped OLEDs

Encouraged by the conspicuous excited state properties of **PIS** and **CNPIS**, we further studied the effect of CN modification on EL performance. Thus, the non-doped OLEDs (**D1** and **D2**) with the configuration of indium tin oxide (ITO)/1,4,5,8,9,11-hexaazatriphenylene-hexacarbonitrile (HATCN, 10 nm)/4,4′-cyclohexylidenebis[*N,N*-bis(4-methylphenyl)benzenamine] (TAPC, 50 nm)/4,4′,4is(4-methylphenyl)benzenamine] (TCTA, 10 nm)/**PIS** or **CNPIS** (20 nm)/1,3,5-tri(m-pyrid-3-yl-phenyl)-benzene (TmPyPB, 40 nm)/lithium fluoride (LiF, 1 nm)/aluminium
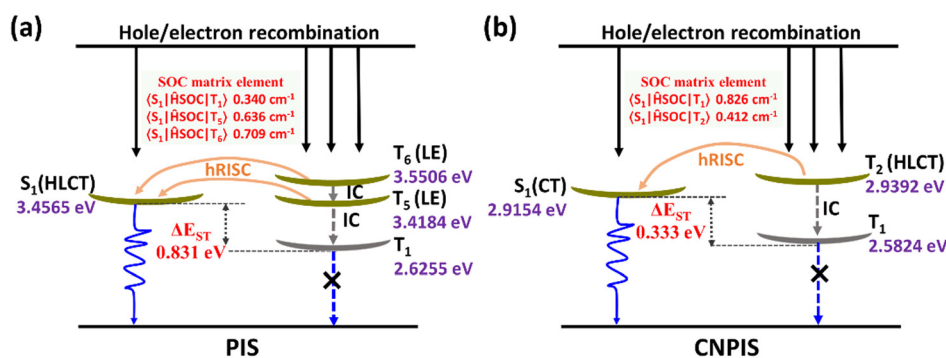

Fig. 3 Probable emission mechanism based on the HLCT state for **PIS** (a) and **CNPIS** (b). S and T are singlet and triplet excited states; LE and CT represent local excited and charge-transfer states; ΔE_{ST} is the singlet–triplet energy splitting between S_1 and T_1; IC and hRISC are the internal conversion and the high-lying reverse intersystem crossing.
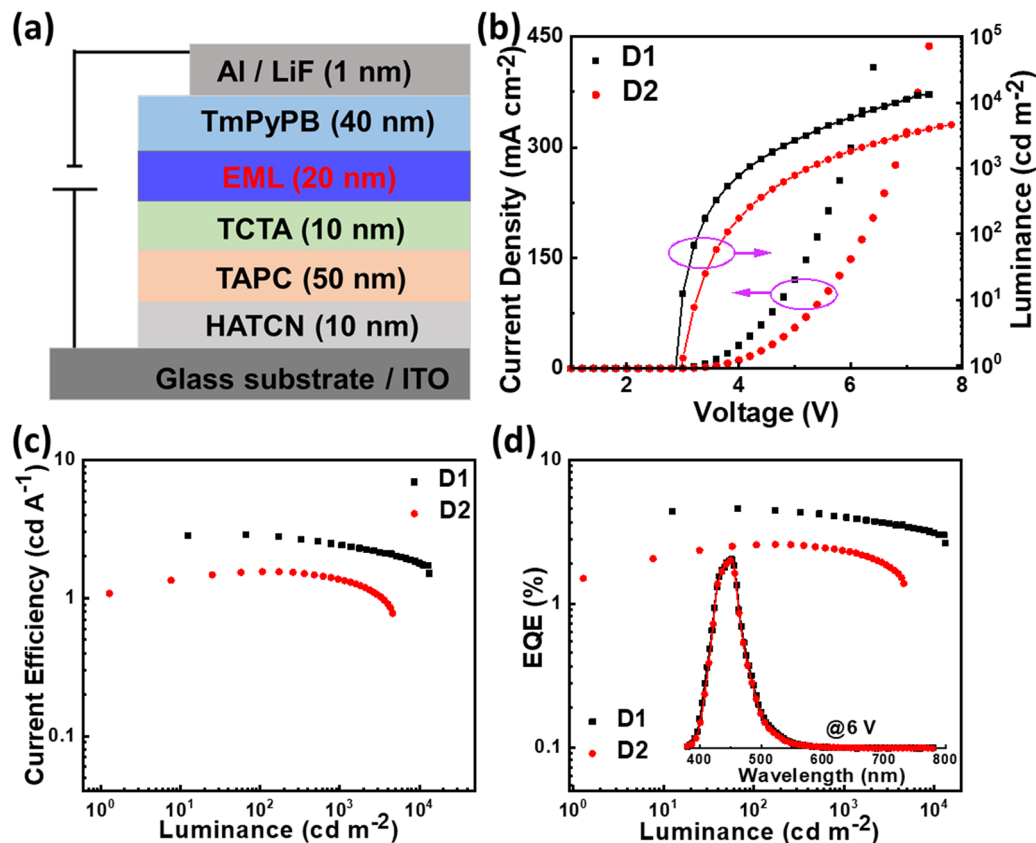
This journal is © The Royal Society of Chemistry and the Chinese Chemical Society 2023

Mater. Chem. Front., 2023, **7**, 85–95 | **89**

Fig. 4 (a) Device configuration diagram. (b) Current−density−voltage−luminance characteristics of the fabricated OLEDs (**D1** and **D2**). (c) Current efficiency *versus* luminance curves of devices **D1** and **D2**. (d) EQE *versus* luminance curves of devices **D1** and **D2**. Insert: Normalized EL spectra at the voltage of 6 V.

(Al, 100 nm) were fabricated and tested. Here, ITO and Al were used as the anode and the cathode; HATCN and LiF served as hole- and electron-injection layers; TAPC and TCTA acted as hole-transporting and exciton-blocking layers; TmPyPB was used as electron-transporting and hole-blocking layers, respectively. Energy level diagram and chemical structures of organic materials used in the devices are shown in Fig. S11 (ESI†). As shown in Fig. 4, Fig. S12, S13, ESI† and Table 2, owing to efficient hole/electron injection, transporting, and recombination, devices **D1** and **D2** realize the low turn-on voltages of 2.9 and 3.0 eV, lower than the values of E_g. As for **D1**, the luminance of 1000 cd m^{-2} and its maximum value (13260 cd m^{-2}) are achieved at the voltages of 4.2 and 7.4 V.

The maximum current efficiency (CE), power efficiency (PE), and EQE are 2.87 cd A^{-1}, 2.95 lm W^{-1}, and 4.59%, respectively. However, device **D2** with CN-modified **CNPIS** as an emissive layer shows a low EQE of 2.59%, which should be attributed to the poor PLQY in its film. More interestingly, both of the devices exhibit stable deep-blue EL spectra with close CIE coordinates of (0.152, 0.067) and (0.153, 0.064) for **D1** and **D2**, further testifying that cyano-substitution in the PI unit has very little effect on emission.

The EUE of OLEDs can be described by eqn (1):

$$\text{EUE} = \frac{\text{EQE}}{\gamma \times \phi_{\text{PLQY}} \times \eta_{\text{OUT}}} \qquad (1)$$

Table 2 Summary of key EL parameters for the devices

Devices	V_{on}^{d} [V]	$\text{CE}_{\text{max/1000}}^{a}$ [cd A^{-1}]	$\text{PE}_{\text{max/1000}}^{a}$ [lm W^{-1}]	$\text{EQE}_{\text{max/1000}}^{a}$ [%]	CIE^{b} (x, y)
D1	2.9/4.2	2.87/2.42	2.95/1.81	4.59/3.99	(0.152, 0.067)
D2	3.0/5.3	1.55/1.36	1.36/0.78	2.59/2.33	(0.153, 0.064)
D3	2.8/3.8	8.37/6.71/5.82^{c}	9.38/5.60	7.08/6.35/5.64^{c}	(0.136, 0.129)
D4	2.9/4.2	7.29/6.43/4.81^{c}	6.78/4.90	5.55/4.95/3.82^{c}	(0.132, 0.170)
Y1	2.7/3.6	87.77/80.26	98.43/70.73	27.30/24.65/22.15^{e}	(0.482, 0.505)
Y2	2.7/3.6	85.17/77.10	95.51/68.10	26.73/24.25/21.90^{e}	(0.497, 0.502)
Y3	2.6/3.5	79.42/72.50	95.91/65.90	25.41/23.43/21.80^{e}	(0.509, 0.494)
W	2.7/3.6	85.85/76.60	96.27/67.60	26.56/23.94/20.08^{e}	(0.459, 0.487)

^{a} Maximum efficiencies and the values taken at 1000 cd m^{-2}. ^{b} Measured at the voltage of 6 V. ^{c} Efficiencies taken at 10 000 cd m^{-2}. ^{d} At 1 and 1000 cd m^{-2}. ^{e} Efficiencies taken at 5000 cd m^{-2}.

Here, ϕ_{PLQY} is the PLQY of the neat film (49.70% for **PIS**; 30.37% for **CNPIS**); γ is the holes and electrons recombination efficiency ($\leq$ 1); η_{out} is the light out-coupling efficiency ($\sim$ 20%). The EUEs can be calculated to be 46.18% and 42.64% for **PIS** and **CNPIS**, exceeding the theoretical limit of traditional fluorescent emitters. Notwithstanding, the phenomenon that cyano-substitution leads to a slight reduction of EUE is distinguished from other reports,[42,51] which may be caused by the special properties of the DBT unit with the third-row sulfur (ZN = 16) atom.

OLEDs based on HLCT-sensitized fluorophore and phosphor

Though the OLEDs (**D1** and **D2**) with **PIS** and **CNPIS** as pure emissive layers have achieved a high EUE of over 25%, the EQEs are less than 5% owing to the poor PLQYs of their neat films. Inspired by the TADF-sensitized fluorescent and TADF-sensitized phosphorescence mechanisms reported by Duan *et al.*, they can simultaneously achieve high efficiency and low roll-off OLEDs even at low doping concentrations.[55–57] HLCT emitters with the separated exciton radiative transition and triplet–singlet conversion channels should be a promising class of host materials for fluorescence and phosphorescence emitters. Taking PIS as an example, in the HLCT-sensitized fluorescence (HSF) mechanism (Fig. 5(a)), electrons and holes recombine on PIS molecules and form singlet and triplet excitons. Triplet excitons can be effectively converted into singlet excitons in the hRISC process. And the singlet excitons transfer their energy to the fluorophore by Förster resonance energy transfer (FET), resulting in emitting light from the fluorophore. As for the HLCT-sensitized phosphorescent (HSP) mechanism (Fig. 5(b)), phosphorescence emission mainly comes from the FET process from the initial and formed singlet excitons up-converted from triplet excitons on the **PIS** host. Some lowest T_1 excitons generated from internal conversion can also transfer their energy to phosphor by Dexter energy transfer (DET) due to the T_1 of **PIS** being higher than that of phosphor.

Based on the above discussion, the blue HSF OLEDs (**D3** and **D4**) with the optimized structure of ITO/HATCN (10 nm)/TAPC (50 nm)/TCTA (10 nm)/**PIS**: 3 wt% BD (20 nm) for **D3** or **CNPIS**: 3 wt% BD (20 nm) for **D4**/TmPyPB (40 nm)/LiF (1 nm)/Al

(100 nm) have been fabricated, where *N,N'*-bis(3-methyl-phenyl)-*N,N'*-bis[3-(9-phenyl-9*H*-fluoren-9-yl)phenyl]-pyrene-1,6-diamine (BD) is a blue conventional fluorescent material with the S_1 and T_1 of 2.68 and 1.81 eV.[58] As shown in Fig. S11c (ESI†), the absorption spectrum of BD (in film state) has large overlaps with the PL spectra of **PIS** and **CNPIS**, implying that the FET process to BD molecules should be very efficient. EL performance is shown in Fig. 6(a) and Fig. S12 (ESI†), and summarized in Table 2. Compared with deep-blue devices (**D1** and **D2**), HLCT-sensitized fluorescent devices realize higher luminance and superior performance with the maximum CE, PE, and EQE of 8.37 cd A^{-1}, 9.38 lm W^{-1}, and 7.08% for **D3**, and 7.29 cd A^{-1}, 6.78 lm W^{-1}, and 5.55% for **D4**. The EQEs have exceeded the limit of 5% in conventional fluorescent OLEDs. More surprisingly, the EQE of device **D3** with **PIS** as the host remains as high as 6.35% at the luminance of 1000 cd m^{-2}, showing a low efficiency roll-off. Even at 10 000 cd m^{-2}, the value remains above 5.6%. The higher EL efficiency achieved in device **D3** may be ascribed to a more effective hRISC process. Meanwhile, devices **D3** and **D4** realize the stable blue emission with the EL peaks at 462 and 468 nm and the narrow full-width at half-maximums (FWHMs) of 42 and 43 nm (Fig. S13c and S12d, ESI†), corresponding to the CIE coordinates of (0.136, 0.129) and (0.132, 0.170) at the voltage of 6 V.

Due to the better EL performance of **PIS**, HSP OLEDs were further fabricated with **PIS** as a host for phosphor. Given the T_1 of **PIS**, yellow phosphorescence emitter iridium(III) bis(4-phenylthieno[3,2-*c*]pyridinato-*N,C*2′)acetylacetonate (PO-01) with the T_1 of 2.2 eV was selected as the dopant. The FET process should be also efficient from **PIS** to PO-01, due to the considerable overlap between the absorption spectrum of PO-01 and the emission spectrum of **PIS**. The optimized device structure is ITO/HATCN (20 nm)/TAPC (50 nm)/TCTA (5 nm)/**PIS**: *XX* wt% PO-01 (15 nm)/1,3,5-tri(phenyl-2-benzimidazolyl)-benzene (TPBi, 40 nm)/LiF (1 nm)/Al (100 nm), where the doping concentrations are 1, 5 and 10 wt% for the devices **Y1**, **Y2** and **Y3**, respectively. The maximum forward-viewing CEs, PEs, and EQEs are 87.77 cd A^{-1}, 98.43 lm W^{-1}, and 27.30% for device **Y1**, 85.15 cd A^{-1}, 95.51 lm W^{-1}, and 26.73% for device **Y2**, 79.42 cd A^{-1}, 95.91 lm W^{-1}, and 25.41% for device **Y3**,
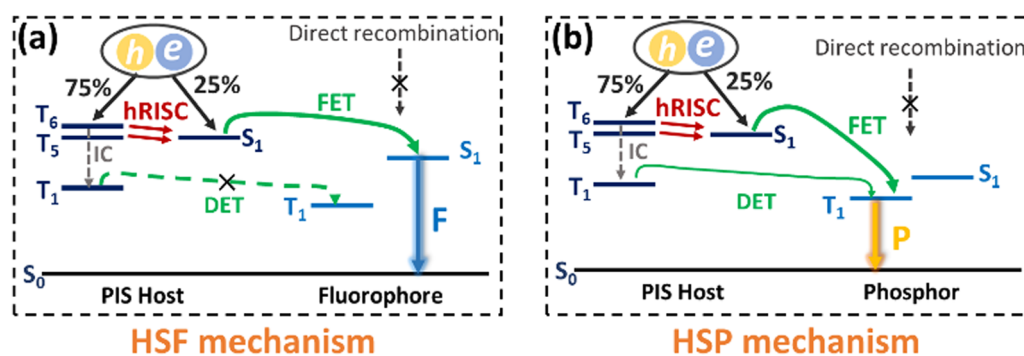
Fig. 5 (a) HLCT–sensitized fluorescence mechanism. (b) HLCT–sensitized phosphorescence mechanism. S and T are singlet and triplet excited states; IC and hRISC are the internal conversion and the high–lying reverse intersystem crossing; FET and DET represent the Förster resonance energy transfer and the Dexter energy transfer, respectively.

This journal is © The Royal Society of Chemistry and the Chinese Chemical Society 2023

Mater. Chem. Front., 2023, **7**, 85–95 | **91**

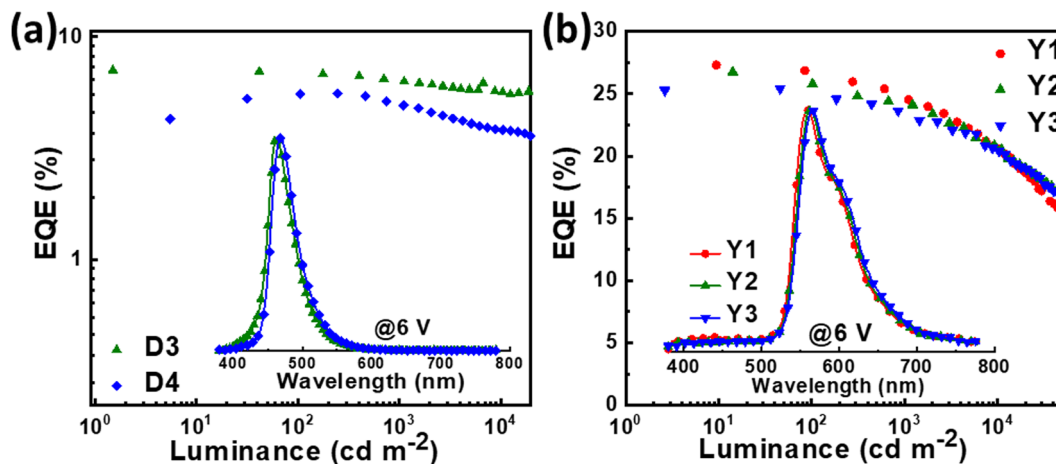Fig. 6 (a) EQE *versus* luminance curves of the blue OLEDs (**D3** and **D4**). Insert: Normalized EL spectra at the voltage of 6 V. (b) EQE *versus* luminance curves of the yellow OLEDs (**Y1**, **Y2** and **Y3**). Insert: Normalized EL spectra at the voltage of 6 V.

respectively. Significantly, the best EL performance (in device **Y1**) is achieved when the low doping concentration of the phosphorescence emitter was merely 1 wt%, which differs from the traditional host-based devices that need a high dopant concentration of phosphors (5–20 wt%) for guaranteeing effective energy transfer from the host to the emitter.[59–61] Such
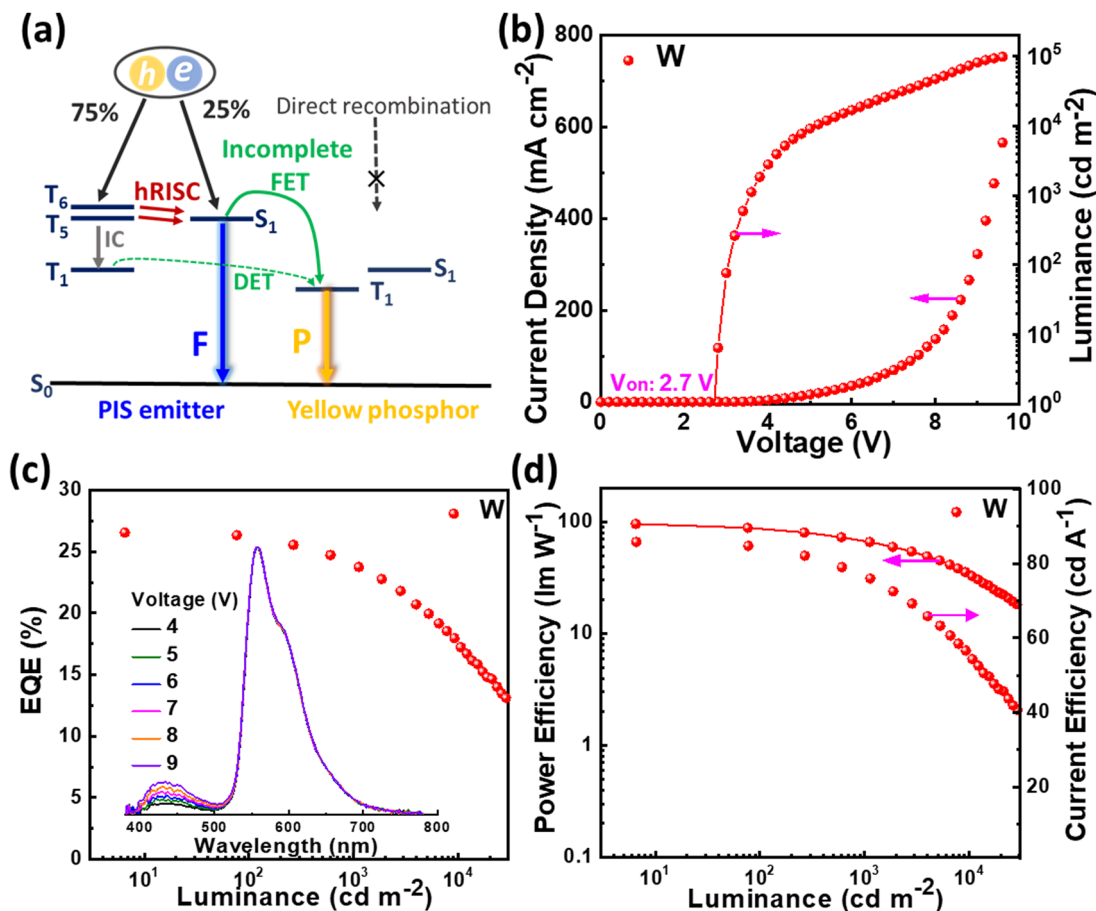

Fig. 7 (a) Emission mechanism of hybrid white device **W** with **PIS** as the host and emitter. (b) Current–density–voltage–luminance characteristics of device **W**. (c) EQE *versus* luminance curves of device **W**. Insert: Normalized EL spectra at different applied voltages. (d) Power efficiency and current efficiency *versus* luminance curves of device **W**.

low phosphor concentration can reduce the high cost of PHOLEDs.[62] In addition, the EQEs of device **Y1** remain as high as 24.65% and 22.15% at the high luminance of 1000 and 5000 cd m^{-2}. These results confirmed that HSP and HSF can be regarded as promising pathways for developing high efficiency and low roll-off OLEDs.

It is known that white light can be generated by integrating blue with yellow emission. In the HSP mechanism, blue emission from the **PIS** host and yellow emission from complementary phosphor can be realized simultaneously by managing the incomplete FET process from the host to phosphor (Fig. 7(a)). Based on this, a simplified hybrid warm-white OLED (**W**) with a single-emissive-layer of **PIS**: 0.5 wt% PO-01 (15 nm) was obtained. As shown in Fig. 7, device **W** achieves the highest forward-viewing CE, PE, and EQE of 85.85 cd A^{-1}, 96.27 lm W^{-1}, and 26.56%. At 1000 cd m^{-2}, the EQE and PE still remain as high as 23.94% and 67.67 lm W^{-1}, respectively. At a voltage of 6 V, the device shows the CIE coordinates of (0.459, 0.487), corresponding to the correlated color temperature of 3227 K. These results confirmed that HSP and HSF can be regarded as the promising pathways to develop high efficiency and low roll-off OLEDs.

Conclusions

In conclusion, we have successfully developed two novel deep-blue HLCT emitters **PIS** and **CNPIS** by managing the anchoring groups at the PI unit. It turns out that cyano modification has an insignificant effect on emission colors but decelerates the hRISC process. Therefore, a higher EQE of 4.59% and CIE coordinates of (0.152, 0.067) are achieved in the non-doped device with **PIS** as an emitter. Based on this, HLCT-sensitized fluorescent and phosphorescent devices with **PIS** as a sensitizer not only realize high efficiencies of 7.08% and 27.30%, 9.38 and 98.43 lm W^{-1} for EQEs and PEs but also exhibit low efficiency roll-off (6.35% and 24.65% @1000 cd m^{-2}), respectively. Furthermore, a hybrid white OLED with **PIS** as the emitter and host shows a PE and an EQE of 96.27 lm W^{-1} and 26.56%, respectively, and retains as high as 67.67 lm W^{-1} and 23.94% at the luminance of 1000 cd m^{-2}. This work may open a new avenue to develop high efficiency and low roll-off OLEDs.

Conflicts of interest

There are no conflicts to declare.

Acknowledgements

Notes and references

1 C. W. Tang and S. A. VanSlyke, Organic electroluminescent diodes, *Appl. Phys. Lett.*, 1987, **51**, 913–915.

2 M. A. Baldo, D. F. O'Brien, Y. You, A. Shoustikov, S. Sibley, M. E. Thompson and S. R. Forrest, Highly efficient phosphorescent emission from organic electroluminescent devices, *Nature*, 1998, **395**, 151–154.

3 H. Uoyama, K. Goushi, K. Shizu, H. Nomura and C. Adachi, Highly efficient organic light-emitting diodes from delayed fluorescence, *Nature*, 2012, **492**, 234–238.

4 Y. Xu, P. Xu, D. Hu and Y. Ma, Recent progress in hot exciton materials for organic light-emitting diodes, *Chem. Soc. Rev.*, 2021, **50**, 1030–1069.

5 C. Du, T. Lu, Z. Cheng, Y. Chang, H. Liu, J. Wang, L. Wan, Y. Lv and P. Lu, Rational molecular design of phenanthroimidazole-based fluorescent materials towards high-efficiency non-doped deep blue OLEDs, *J. Mater. Chem. C*, 2022, **10**, 14186–14193.

6 J. Zhao, B. Liu, Z. Wang, Q. Tong, X. Du, C. Zheng, H. Lin, S. Tao and X. Zhang, EQE climbing over 6% at high brightness of 14 350 cd m^{-2} in deep-blue OLEDs based on hybridized local and charge-transfer fluorescence, *ACS Appl. Mater. Interfaces*, 2018, **10**, 9629–9637.

7 F. Liu, Z. Cheng, L. Wan, L. Gao, Z. Yan, D. Hu, L. Ying, P. Lu and Y. Ma, Anthracene-based emitters for highly efficient deep blue organic light-emitting diodes with narrow emission spectrum, *Chem. Eng. J.*, 2021, **426**, 131351.

8 H. L. Lee, S. O. Jeon, I. Kim, S. C. Kim, J. Lim, J. Kim, S. Park, J. Chwae, W.-J. Son, H. Choi and J. Y. Lee, Multiple-resonance extension and spin-vibronic-coupling-based narrowband blue organic fluorescence emitters with over 30% quantum efficiency, *Adv. Mater.*, 2022, **34**, 2202464.

9 F. Huang, K. Wang, Y.-Z. Shi, X.-C. Fan, X. Zhang, J. Yu, C.-S. Lee and X.-H. Zhang, Approaching efficient and narrow RGB electroluminescence from D–A-type TADF emitters containing an identical multiple resonance backbone as the acceptor, *ACS Appl. Mater. Interfaces*, 2021, **13**, 36089–36097.

10 X. Cai, J. Xue, C. Li, B. Liang, A. Ying, Y. Tan, S. Gong and Y. Wang, Achieving 37.1% green electroluminescent efficiency and 0.09 ev full width at half maximum based on a ternary boron-oxygen-nitrogen embedded polycyclic aromatic system, *Angew. Chem. Int. Ed.*, 2022, **61**, e202200337.

11 F. Liu, Z. Cheng, L. Wan, Z. Feng, H. Liu, H. Jin, L. Gao, P. Lu and W. Yang, Highly efficient multi-resonance thermally activated delayed fluorescence material with a narrow full width at half-maximum of 0.14 eV, *Small*, 2022, **18**, 2106462.

12 Y. Chen, J. Zhu, Y. Wu, J. Yao, D. Yang, X. Qiao, Y. Dai, Q. Tong and D. Ma, Highly efficient fluorescence/phosphorescence hybrid white organic light-emitting devices based on a bipolar blue emitter to precisely control charges and excitons, *J. Mater. Chem. C*, 2020, **8**, 7543–7551.

13 S. Ying, W. Liu, L. Peng, Y. Dai, D. Yang, X. Qiao, J. Chen, L. Wang and D. Ma, A Promising multifunctional deep-blue

This journal is © The Royal Society of Chemistry and the Chinese Chemical Society 2023

Mater. Chem. Front., 2023, **7**, 85–95 | **93**

fluorophor for high-performance monochromatic and hybrid white OLEDs with superior efficiency/color stability and low efficiency roll-off, *Adv. Opt. Mater.*, 2022, **10**, 2101920.

14 S.-C. Dong, L. Zhang, J. Liang, L.-S. Cui, Q. Li, Z.-Q. Jiang and L.-S. Liao, Rational design of dibenzothiophene-based host materials for PHOLEDs, *J. Phys. Chem. C*, 2014, **118**, 2375–2384.

15 R. Huang, N. A. Kukhta, J. S. Ward, A. Danos, A. S. Batsanov, M. R. Bryce and F. B. Dias, Balancing charge-transfer strength and triplet states for deep-blue thermally activated delayed fluorescence with an unconventional electron rich dibenzothiophene acceptor, *J. Mater. Chem. C*, 2019, **7**, 13224–13234.

16 X.-Y. Liu, F. Liang, L.-S. Cui, X.-D. Yuan, Z.-Q. Jiang and L.-S. Liao, Effective host materials for blue/white organic light-emitting diodes by utilizing the twisted conjugation structure in 10-phenyl-9,10-dihydroacridine block, *Chem. – Asian J.*, 2015, **10**, 1402–1409.

17 Y.-J. Na, W. Song, J. Y. Lee and S.-H. Hwang, Synthesis of dibenzothiophene-based host materials and their blue phosphorescent device performances, *Org. Electron.*, 2015, **22**, 92–97.

18 C. W. Lee and J. Y. Lee, Structure-property relationship of pyridoindole-type host materials for high-efficiency blue phosphorescent organic light-emitting diodes, *Chem. Mater.*, 2014, **26**, 1616–1621.

19 J. H. Kim, S. H. Han and J. Y. Lee, Dibenzothiophene derived hosts with CN substituted carbazole for blue thermally activated delayed fluorescent organic light-emitting diodes, *Synth. Met.*, 2017, **232**, 152–158.

20 L. Ding, W.-Z. Fo, X.-Y. Liu, H. Chen, F. Igbari, J.-H. Wu and Z.-Q. Jiang, Highly efficient green phosphorescent organic light-emitting diodes based on tetraphenyl silicon derivative host materials, *Org. Electron.*, 2020, **78**, 105581.

21 S.-C. Dong, C.-H. Gao, X.-D. Yuan, L.-S. Cui, Z.-Q. Jiang, S.-T. Lee and L.-S. Liao, Novel dibenzothiophene based host materials incorporating spirobifluorene for high-efficiency white phosphorescent organic light-emitting diodes, *Org. Electron.*, 2013, **14**, 902–908.

22 S. H. Jeong and J. Y. Lee, Dibenzothiophene derivatives as host materials for high efficiency in deep blue phosphorescent organic light emitting diodes, *J. Mater. Chem.*, 2011, **21**, 14604–14609.

23 L. Ding, J.-N. Wang, X.-Y. Liu, H. Chen, F. Igbari and L.-S. Liao, Dibenzothiophene, dibenzofuran and pyridine substituted tetraphenyl silicon derivatives hosts for green phosphorescent organic light-emitting diodes, *Org. Electron.*, 2019, **71**, 258–265.

24 S. K. Shin, S. Y. Byeon, S. H. Han and J. Y. Lee, novel host materials based on dibenzothiophene and carbazolylcarbazole for extended lifetime in blue phosphorescent organic light-emitting diodes, *Adv. Opt. Mater.*, 2018, **6**, 1701007.

25 C. Han, Z. Zhang, H. Xu, S. Yue, J. Li, P. Yan, Z. Deng, Y. Zhao, P. Yan and S. Liu, Short-axis substitution approach selectively optimizes electrical properties of dibenzothiophene-based phosphine oxide hosts, *J. Am. Chem. Soc.*, 2012, **134**, 19179–19188.

26 S. Y. Byeon, S. H. Han and J. Y. Lee, Carbazole-dibenzothiophene core as a building block of host materials for blue phosphorescent organic light-emitting diodes, *Dyes Pigm.*, 2018, **155**, 114–120.

27 F. Wang, J. Sun, M. Liu, H. Shi, H. Ma, W. Ye, H. Wang, H. Zhang, Z. An and W. Huang, D–A–D-type bipolar host materials with room temperature phosphorescence for high-efficiency green phosphorescent organic light-emitting diodes, *J. Mater. Chem. C*, 2020, **8**, 1871–1878.

28 Y. J. Kang and J. Y. Lee, P-170: Synthesis and device performances of high triplet energy electron transport materials, *Dig. Tech. Pap. – Soc. Inf. Disp. Int. Symp.*, 2016, **47**, 1757–1759.

29 H. Fukagawa, T. Shimizu, H. Kawano, S. Yui, T. Shinnai, A. Iwai, K. Tsuchiya and T. Yamamoto, Novel Hole-transporting materials with high triplet energy for highly efficient and stable organic light-emitting diodes, *J. Phys. Chem. C*, 2016, **120**, 18748–18755.

30 H. Fukagawa, T. Shimizu, Y. Kiribayashi, Y. Osada, T. Kamada, T. Yamamoto, N. Shimidzu and T. Kurita, Molecular design of hole-transporting material for efficient and stable green phosphorescent organic light-emitting diodes, *Appl. Phys. Lett.*, 2013, **103**, 143306.

31 S. Chen, Y. Wu, Y. Zhao and D. Fang, Deep blue organic light-emitting devices enabled by bipolar phenanthro[9,10-*d*]imidazole derivatives, *RSC Adv.*, 2015, **5**, 72009–72018.

32 J. Ye, Y. Gao, L. He, T. Tan, W. Chen, Y. Liu, Y. Wang and G. Ning, Efficient blue-emitting molecules by incorporating sulfur-containing moieties into triarylcyclopentadiene: Synthesis, crystal structures and photophysical properties, *Dyes Pigm.*, 2016, **124**, 145–155.

33 J. Guo, X.-L. Li, H. Nie, W. Luo, S. Gan, S. Hu, R. Hu, A. Qin, Z. Zhao, S.-J. Su and B. Z. Tang, Achieving high-performance nondoped OLEDs with extremely small efficiency roll-off by combining aggregation-induced emission and thermally activated delayed fluorescence, *Adv. Funct. Mater.*, 2017, **27**, 1606458.

34 J. Guo, X.-L. Li, H. Nie, W. Luo, R. Hu, A. Qin, Z. Zhao, S.-J. Su and B. Z. Tang, Robust luminescent materials with prominent aggregation-induced emission and thermally activated delayed fluorescence for high-performance organic light-emitting diodes, *Chem. Mater.*, 2017, **29**, 3623–3631.

35 J. Tang, Y. Sun, Q. Tang and Y. Sun, Molecular engineering of A–D–D–A dual-emitting-cores emitters with thermally activated delayed fluorescence and aggregation-induced emission characteristics, *Org. Electron.*, 2021, **96**, 106199.

36 C. Xia, X. Wang, J. Lin, W. Jiang, Y. Ni and W. Huang, Organic light-emitting devices (OLED) based on new triphenylamine derivatives, *Synth. Met.*, 2009, **159**, 194–200.

37 Y. Sim, H. Lee, J. Park, D. Shin, M. Park and K.-Y. Kay, Synthesis and electroluminescence property of pyrene derivatives including dibenzothiophene and imidazole moiety, *J. Nanosci. Nanotechnol.*, 2019, **19**, 4710–4714.

38 K. H. Lee, J. H. Seo, Y. K. Kim and S. S. Yoon, *N,N*-(Diphenylamino)fluorenylstyrene derivatives with the

94 | *Mater. Chem. Front.*, 2023, **7**, 85–95

This journal is © The Royal Society of Chemistry and the Chinese Chemical Society 2023

various heteroatom-containing moieties for blue organic light-emitting diodes, *J. Nanosci. Nanotechnol.*, 2013, **13**, 1808–1811.

39 L. Yao, S. Sun, S. Xue, S. Zhang, X. Wu, H. Zhang, Y. Pan, C. Gu, F. Li and Y. Ma, Aromatic S-heterocycle and fluorene derivatives as solution-processed blue fluorescent emitters: Structure-property relationships for different sulfur oxidation states, *J. Phys. Chem. C*, 2013, **117**, 14189–14196.

40 X. Tang, T. Shan, Q. Bai, H. Ma, X. He and P. Lu, Efficient deep-blue electroluminescence based on phenanthroimidazole-dibenzothiophene derivatives with different oxidation states of the sulfur atom, *Chem. – Asian J.*, 2017, **12**, 552–560.

41 X. Tang, Q. Bai, T. Shan, J. Li, Y. Gao, F. Liu, H. Liu, Q. Peng, B. Yang, F. Li and P. Lu, Efficient nondoped blue fluorescent organic light-emitting diodes (OLEDs) with a high external quantum efficiency of 9.4% @ 1000 cd m^{-2} based on phenanthroimidazole-anthracene derivative, *Adv. Funct. Mater.*, 2018, **28**, 1705813.

42 S. Zhang, L. Yao, Q. Peng, W. Li, Y. Pan, R. Xiao, Y. Gao, C. Gu, Z. Wang, P. Lu, F. Li, S. Su, B. Yang and Y. Ma, Achieving a significantly increased efficiency in nondoped pure blue fluorescent OLED: A quasi-equivalent hybridized excited state, *Adv. Funct. Mater.*, 2015, **25**, 1755–1762.

43 S. Ying, J. Lv, Y. Li, Y. Huo, Y. Liu, D. Ma, L. Peng and S. Yan, A large-scale deep-blue tetraphenylbenzene-bridged hybridized local and charge transfer fluorophore exhibiting small efficiency roll-off and low amplified spontaneous emission threshold, *Mater. Chem. Front.*, 2022, **6**, 2085–2094.

44 Z. Gao, Z. Wang, T. Shan, Y. Liu, F. Shen, Y. Pan, H. Zhang, X. He, P. Lu, B. Yang and Y. Ma, High-efficiency deep blue fluorescent emitters based on phenanthro 9,10-d imidazole substituted carbazole and their applications in organic light emitting diodes, *Org. Electron.*, 2014, **15**, 2667–2676.

45 K. A. Zachariasse, T. v d Haar, A. Hebecker, U. Leinhos and W. Kuhnle, Intramolecular charge transfer in aminobenzonitriles: Requirements for dual fluorescence, *Pure Appl. Chem.*, 1993, **65**, 1745–1750.

46 H. Zhou, R. Wang, S. T. Zhang, W. Cui, S. Ying, Q. Sun, B. Yang, S. Xue, W. Yang and Y. Ma, Highly efficient blue-emissive electroluminescence: Nondestructive color regulation effect of orthogonal cyano-substitution in hybrid locally-excited and charge-transfer (HLCT) backbone emitters, *Mater. Today Chem.*, 2022, **24**, 100785.

47 J. Chen, H. Liu, J. Guo, J. Wang, N. Qiu, S. Xiao, J. Chi, D. Yang, D. Ma, Z. Zhao and B. Z. Tang, Robust Luminescent molecules with high-level reverse intersystem crossing for efficient near ultraviolet organic light-emitting diodes, *Angew. Chem., Int. Ed.*, 2022, **61**, e202116810.

48 Y. Liu, X. Man, Q. Bai, H. Liu, P. Liu, Y. Fu, D. Hu, P. Lu and Y. Ma, Highly efficient blue organic light-emitting diode based on a pyrene[4,5-d]imidazole-pyrene molecule, *CCS Chem.*, 2022, **4**, 214–227.

49 S. Xiao, S.-T. Zhang, Y. Gao, X. Yang, H. Liu, W. Li and B. Yang, Efficient and stable deep-blue narrow-spectrum electroluminescence based on hybridized local and charge-transfer (HLCT) state, *Dyes Pigm.*, 2021, **193**, 109482.

50 H. Zhang, B. Zhang, Y. Zhang, Z. Xu, H. Wu, P.-A. Yin, Z. Wang, Z. Zhao, D. Ma and B. Z. Tang, A Multifunctional blue-emitting material designed via tuning distribution of hybridized excited-state for high-performance blue and host-sensitized OLEDs, *Adv. Funct. Mater.*, 2020, **30**, 2002323.

51 H. Zhang, J. Zeng, W. Luo, H. Wu, C. Zeng, K. Zhang, W. Feng, Z. Wang, Z. Zhao and B. Z. Tang, Synergistic tuning of the optical and electrical performance of AIEgens with a hybridized local and charge-transfer excited state, *J. Mater. Chem. C*, 2019, **7**, 6359–6368.

52 J. U. Kim, I. S. Park, C.-Y. Chan, M. Tanaka, Y. Tsuchiya, H. Nakanotani and C. Adachi, Nanosecond-time-scale delayed fluorescence molecule for deep-blue OLEDs with small efficiency rolloff, *Nat. Commun.*, 2020, **11**, 1765.

53 M. A. El-Sayed, Spin–orbit coupling and the radiationless processes in nitrogen heterocyclics, *J. Chem. Phys.*, 1963, **38**, 2834–2838.

54 R. Chen, Y. Tang, Y. Wan, T. Chen, C. Zheng, Y. Qi, Y. Cheng and W. Huang, Promoting singlet/triplet exciton transformation in organic optoelectronic molecules: Role of excited state transition configuration, *Sci. Rep.*, 2017, **7**, 6225.

55 M. Cai, D. Zhang and L. Duan, High Performance thermally activated delayed fluorescence sensitized organic light-emitting diodes, *Chem. Rec.*, 2019, **19**, 1611–1623.

56 D. Zhang, L. Duan, C. Li, Y. Li, H. Li, D. Zhang and Y. Qiu, High-efficiency fluorescent organic light-emitting devices using sensitizing hosts with a small singlet–triplet exchange energy, *Adv. Mater.*, 2014, **26**, 5050–5055.

57 D. Zhang, L. Duan, D. Zhang, J. Qiao, G. Dong, L. Wang and Y. Qiu, Extremely low driving voltage electrophosphorescent green organic light-emitting diodes based on a host material with small singlet–triplet exchange energy without p- or n-doping layer, *Org. Electron.*, 2013, **14**, 260–266.

58 H. Lim, H. J. Cheon, G. S. Lee, M. Kim, Y.-H. Kim and J.-J. Kim, Enhanced triplet–triplet annihilation of blue fluorescent organic light-emitting diodes by generating excitons in trapped charge-free regions, *ACS Appl. Mater. Interfaces*, 2019, **11**, 48121–48127.

59 H. Sasabe, H. Nakanishi, Y. Watanabe, S. Yano, M. Hirasawa, Y.-J. Pu and J. Kido, Extremely low operating voltage green phosphorescent organic light-emitting devices, *Adv. Funct. Mater.*, 2013, **23**, 5550–5555.

60 H. Liu, Q. Bai, L. Yao, D. Hu, X. Tang, F. Shen, H. Zhang, Y. Gao, P. Lu, B. Yang and Y. Ma, Solution-processable hosts constructed by carbazole/PO substituted tetraphenylsilanes for efficient blue electrophosphorescent devices, *Adv. Funct. Mater.*, 2014, **24**, 5881–5888.

61 X.-D. Yuan, J. Liang, Y.-C. He, Q. Li, C. Zhong, Z.-Q. Jiang and L.-S. Liao, A rational design of carbazole-based host materials with suitable spacer group towards highly-efficient blue phosphorescence, *J. Mater. Chem. C*, 2014, **2**, 6387–6394.

62 D. Zhang, L. Duan, D. Zhang and Y. Qiu, Towards ideal electrophosphorescent devices with low dopant concentrations: The key role of triplet up-conversion, *J. Mater. Chem. C*, 2014, **2**, 8983–8989.

This journal is © The Royal Society of Chemistry and the Chinese Chemical Society 2023

Mater. Chem. Front., 2023, **7**, 85–95 | **95**